

# Numerical analysis on the influence of device parameters on the performance of quantum cascade lasers

P. ASHOK\*, M. GANESH MADHAN

*Department of Electronics Engineering, Madras Institute of Technology Campus, Anna University, Chennai, India, 600 044*

---

A detailed numerical analysis of mid infrared quantum cascade lasers (QCLs) is carried out by solving the standard two-level rate equations. This analysis accounts for the influence of optical mode confinement factor ( $\Gamma$ ), spontaneous emission factor ( $\beta$ ) and Reflectivities (R) of the facets on the dynamics of the mid-infrared QCL. The dependence of threshold current, Steady state photon number, electron number in different levels, built-up time on the device parameters is investigated thoroughly. This analysis aids in determining optimum values of device parameters and operating conditions.

(Received October 13, 2014; accepted April 5, 2016)

*Keywords:* Quantum Cascade Lasers (QCLs), Tera Hertz (THz), Numerical Simulation, Rate Equations, Spontaneous Emission Factor

---

## 1. Introduction

Quantum Cascade Lasers (QCLs) are unipolar semiconductor devices that utilize inter sub-band transitions in a repetition of identical coupled multi-quantum well structures. They are small-size, high-efficiency semiconductor sources of radiation in the mid infrared and terahertz wave bands. Other features include electrical pumping, tuneability and ease of integration. QCLs were first demonstrated by Bell Laboratories on an InP substrate [1]. Various approaches for the QCL design such as the three quantum well active region method [2],[3], super lattice active region design [4],[5], two phonons active region design [6] and the bound to continuum design [7],[8] are reported. Injector doping [9] is an important parameter which can influence the performance of a QCL. A temperature dependent Gain modeling is done [10] to account for the influence of temperature on the photoelectric properties of QCLs.

While the compact theoretical models are accurate, these methods become computationally intense due to the numerical nature of all the parameters. Due to the complex nature of Green's function formalism and Monte Carlo Simulation, the model of self consistent rate equations are used to formulate the model for a high performance QCL [11], with lower threshold current and larger slope efficiency. This can improve the operational temperature of the THz QCLs. The direct intensity modulation response of QCLs can be studied either from a three level model or a simplified two level model. But the former method is computationally intensive and hence a two level model is preferred [12]. It has been predicted that the modulation bandwidth increases linearly with optical power and saturates to a value which is determined by the photon life time. Delay time in QCLs [13],[14] results in spontaneous emission induced intensity noise in the output optical power.

Another factor is the turn on delay time, which is the time needed for the laser to reach threshold and it depends on the phonon scattering times and the injection current. From the literature, it is observed that in-depth study on the impact of device parameters is well documented in the case of double heterojunction lasers by Tucker et al. [15], bisection quantum well laser diodes by Piramasubramanian et al. [16] and in bistable laser diodes by Ganesh Madhan et al. [17]. However, detailed investigations on the influence of the device parameters on the performance of QCLs still remain sparse. Till date, only the time evolution analysis of Photon number for variation in spontaneous emission factor on the device parameters has been carried out [13-14]. These findings also do not account for the behaviour of built-up time, rise time, delay time and their dependence on  $\beta$ . Hence, we investigate the transient and steady state device behaviour for various values of mode confinement factor ( $\Gamma$ ), spontaneous emission factor ( $\beta$ ) and facet reflectivities for a QCL operating at  $9\mu\text{m}$ . The device considered for the work has a threshold current of 1.1108A [13-14] and is operated with a bias current of  $2.5I_{\text{th}}$ . Considering the results of Hamadou et al. [13] as our reference, the influence of the above said parameters are studied in detail in this paper. The rate equations are solved numerically by Runge-Kutta method using ODE solver in MATLAB.

The paper is organized as follows. Section II explains the simplified two level model used for the numerical simulation of QCL. Section III provides the analysis on the time evolution of the electron distribution in different levels and the photon number within the cavity, for the parametric variation in  $\Gamma$ ,  $\beta$  and R ( $R_1=R_2$ ). Section IV concludes our findings.

## 2. Rate Equations of a midinfrared QC laser

### 2.1 Improved two level model [12]

The three level model is shown in Fig. 1a where  $\tau_n$  denotes the electron lifetime for transitions between levels 3 and 2. The structure of a typical QCL is shown in Fig. 1b.

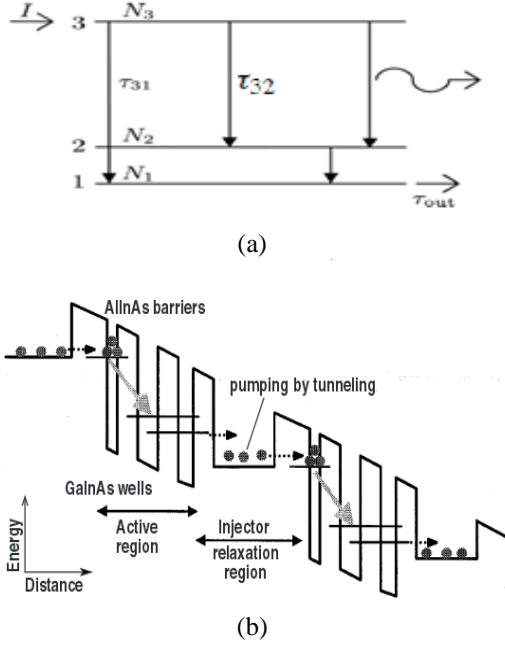


Fig. 1. (a) Three Level Model in Conduction Well [13]  
(b) Band Structure of a typical QCL.

It also includes non-radiative transitions and spontaneous emissions i.e.,

$$\frac{1}{\tau_n} = \frac{1}{\tau_{32}} + \frac{1}{\tau_{sp}} \quad (1)$$

where  $\tau_{32}$  represents the non radiative transition lifetime between levels 3 and 2 and  $\tau_{sp}$  is the spontaneous emission lifetime. Eq. (2) is needed to maintain current continuity. For other cases, the terms involving  $\tau_{32}$  can be ignored to give an improved two level model which is shown in Fig. 2.

$$\frac{dN_1}{dt} = \frac{N_2}{\tau_{21}} + \frac{N_3}{\tau_{31}} - \frac{N_1}{\tau_{out}} \quad (2)$$

In Eq. (2),  $N_1$  is the electron number in energy level 1 and  $\tau_{31}$  and  $\tau_{21}$  are the electron life times representing non radiative transitions between levels 3 and 1, and 2 and 1, respectively.

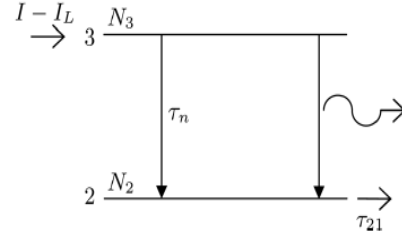


Fig. 2. Improved Two Level Model

The term  $\tau_{31}$  which was neglected in earlier two level models as in [14] is incorporated in the present model into a current  $I_L$  which represents the non-radiative recombination current as in Eq. 3.

$$I_L = \frac{eN_3}{\tau_{31}} \quad (3)$$

The only difference between Fig. 1 and Fig. 2 are the current  $I_L$  and the replacement of  $\tau_{out}$  by  $\tau_{21}$ . The improved two level rate equations as in [13] are given by

$$\frac{dN_3}{dt} = \frac{I}{e} - \frac{N_3}{\tau_3} - G(N_3 - N_2)P \quad (4)$$

$$\frac{dN_2}{dt} = \left( \frac{1}{\tau_{32}} + \frac{1}{\tau_{sp}} \right) N_3 - \frac{N_2}{\tau_{21}} + G(N_3 - N_2)P \quad (5)$$

$$\frac{dP}{dt} = GN(N_3 - N_2)P + N\beta \frac{N_3}{\tau_{sp}} - \frac{P}{\tau_p} \quad (6)$$

where  $N_2$  and  $N_3$  are the electron numbers in level 2 and 3 respectively;  $P$  is the photon number;  $I$  is the injected current,  $G$  is the gain coefficient per stage and given by

$$G = \Gamma \frac{c' \sigma_{32}}{V} \quad (7)$$

$\Gamma$  is the optical confinement factor,  $c' = c/n_{eff}$  where  $n_{eff}$  and  $c$  are the effective refractive index of the cavity and the speed of light in vacuum, respectively.  $\sigma_{32}$  stands for the stimulated emission cross section between the upper and lower levels.  $V$  is the volume of the active region given by  $V = NWLL_p$ , where  $W$  and  $L$  are the lateral length and width of the cavity,  $N$  and  $L_p$  stands for the number of stages and length of each of the stage. Each period or stage contains a barrier and quantum well(s). The barriers are widely spaced and characterized by low refractive index, whereas the active region has quantum wells and higher value of refractive index. This arrangement provides wave guiding of light in the active region. Usually, a number of alternating structures of active region and injector/relaxation regions are stacked. When an electron is injected in to the active region, photons are produced in each period thereby generating more photons, beyond threshold [19].  $\beta$  represents the fraction of spontaneous emission entering the lasing mode. The total carrier lifetime ( $\tau_3$ ) is given by the following expression

$$\frac{1}{\tau_3} = \frac{1}{\tau_{31}} + \frac{1}{\tau_{32}} + \frac{1}{\tau_{sp}} \quad (8)$$

### 3. Simulation results

The rate equations depicted in Eq. (4) to (6) are solved recursively to obtain steady state and transient responses using ODE Solver in MATLAB. The device parameters used in the analysis are listed in Table 1. The photon number (P) is evaluated for bias current (I) varying from 0-2A which provides the light current characteristics under dc conditions. The results match well with references [13-14] thereby validating our simulation.

Table 1. Parameters Of QCL [13],[14]

Parameter	Value
Wavelength, $\lambda$	9.0 $\mu\text{m}$
Number of Gain stages, N	48
$\tau_{32}$	2.1ps
$\tau_{31}$	4.2ps
$\tau_{21}$	0.3ps
$\tau_p$	3.36ps
$\tau_{sp}$	35.5ns
Mirror loss coefficient, $\alpha_m$	12.4 (cm) <sup>-1</sup>
Gain coefficient per stage	744 s <sup>-1</sup>
Spontaneous Emission Factor, $\beta$	2x10 <sup>-3</sup>
Threshold Current $I_{th}$	1.1108 A
Lateral Width of the Cavity, W	34 $\mu\text{m}$
Lateral Length of the Cavity, L	1mm
Length of each stage, $L_p$	45nm
Reflectivities ( $R_1=R_2$ )	0.29
Effective Refractive index of the cavity, $n_{eff}$	3.27
Optical Confinement Factor, $\Gamma$	0.32

The Threshold current matches well with the value of 1.1108A as obtained by Kelvin et al. [14]. The photon number increases linearly above the threshold current as in the case of normal semiconductor lasers. The output optical power can be computed from the photon number as,

$$P_{opt} = P(1-R)h\left(\frac{c}{\lambda}\right)\left(\frac{c}{n}\right)\left(\frac{1}{L}\right) \quad (9)$$

Fig. 3 shows the optical power current characteristic obtained in DC simulation. It also shows the variation of population difference with respect to the bias current. Crosses in the plots represent simulation results which match well with Ref [14].

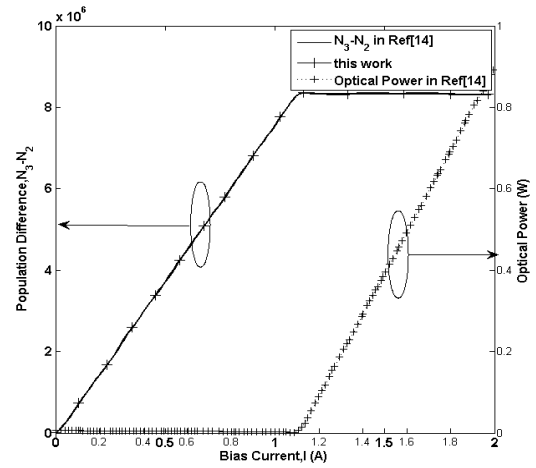


Fig. 3. Population Difference-Current and Optical Power-Current characteristics

The pulse response of QCL's provided in [14] have been re-simulated to confirm the basic transient and steady state responses and also to fix our simulation conditions. When a step current of  $1.5I_{th}$  is applied to QCL with zero initial conditions, the number of electrons at level 3 rises rapidly and maintains a steady state value of  $1.2 \times 10^7$  electrons, it then slowly starts to decrease and settle down at  $1 \times 10^7$  electrons, as the photon number increases. Built-up time of a laser is defined as the period where the number of electrons remains at a steady state value and the photon number is very small as defined in [14]. Delay time of a laser is defined as the time required by the photon number to reach 10% of its steady state value from a zero initial condition on any step input current.

The delay time can be thought of a sum of two components namely turn on delay time needed for the population inversion to reach its threshold value, and the built up time. The simulation results are compared with the numerical results in Fig. 4 and a good agreement is obtained with Ref [14].

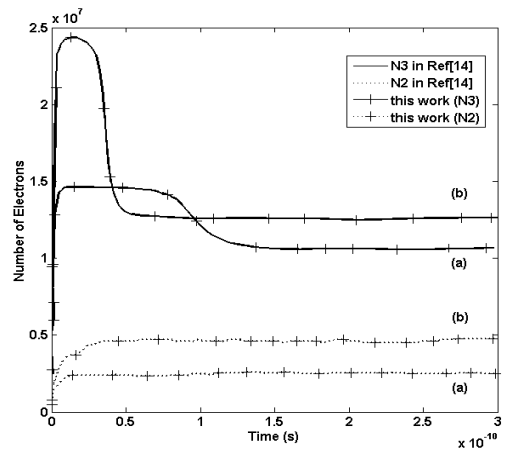


Fig. 4. Comparison of time evolution curves for number of electrons in level 3 and 2 for the bias current a)  $I/I_{th}=1.5$  and b)  $I/I_{th}=2.5$ .

It is observed that the delay time, built-up time reduces as the pulse current is increased above the threshold current. The electron density  $N_3$  shrinks towards the left which indicates the desired reduction in the delay time, rise time and built-up time. The graphs involving built-up time, delay time and turn-on-delay time are also found to be in good agreement with [14]. The photon number increases slightly while the population inversion begins and then reaches its stable stationary value, which is similar to that observed in conventional semiconductor lasers as in Ref [15].

### 3.1 Influence of spontaneous emission factor ( $\beta$ )

The spontaneous emission factor  $\beta$  is an important parameter for the characterization of semiconductor light emitting devices. It is defined as the ratio of rate of spontaneous emission contributed to the output to the total spontaneous emission rate. The spontaneous emission factor  $\beta$  depends on the lateral guiding mechanism and is enhanced for gain guided lasers. It also depends on Temperature, spontaneous emission bandwidth and cavity volume. In practice,  $\beta$  is treated as a fitting parameter in rate equations and its variation on the device characteristics are reported in literature [18],[13]. Hence, in order to analyze the influence of device parameters on the performance of QCL, various values of  $\beta$ , possible in a QCL case, have been used in the analysis. From the literature [13], the impact of  $\beta$  is seen mainly on the time trajectory of the optical power. It can have values between  $10^{-2}$  and  $10^{-3}$  as in Ref [14]. The dynamic trajectory followed by the system to reach its state of oscillation depends crucially on the phonon scattering times and the injection current density. It also depends strongly on the spontaneous emission factor;  $\beta$ . Fig. 5 shows the time evolution of the photon number for different values of  $\beta$ .

It may be noted from the Fig. 5 that, as the value of  $\beta$  is increased, the graph shifts leftward causing a reduction in built-up time and turn-on delay time. It is worthwhile to stress the strong decrease of turn-on delay time as the injected current  $I$  increases from  $I_{th}$  onwards.

#### 3.1.1 DC characteristics

The bias current ( $I$ ) to the QCL is varied from 0-2A and the optical power ( $P$ ) is calculated. The DC characteristic curve of the device is obtained by plotting  $I$  vs  $P$ .

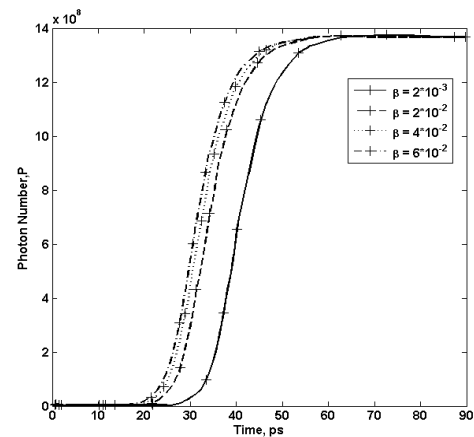
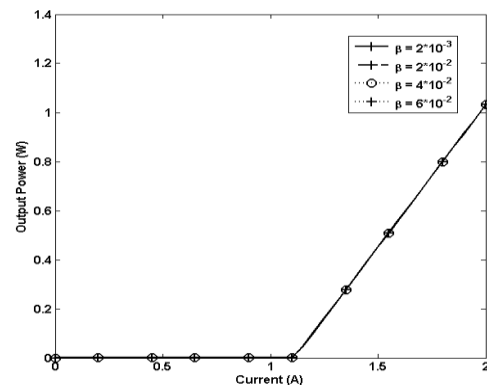
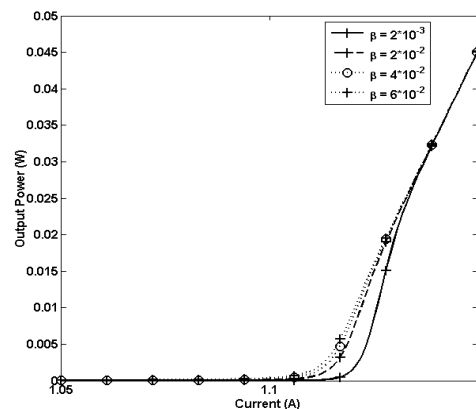


Fig. 5. Time evolution of the number of photons for different spontaneous emission factors

It is observed in Fig. 6a that the optical power increased linearly after the Threshold current of 1.1108A which is similar in the case of conventional semiconductor lasers. But when the curve is analysed around the threshold current with more precision and data points, that the P-I characteristics exhibits a non linearity in the region around the threshold current. As the value of  $\beta$  is increased, the slope ( $dP/dI$ ) reduces from 1.4504 W/A to 1.2518 W/A which can be seen in Fig. 6b.



(a)

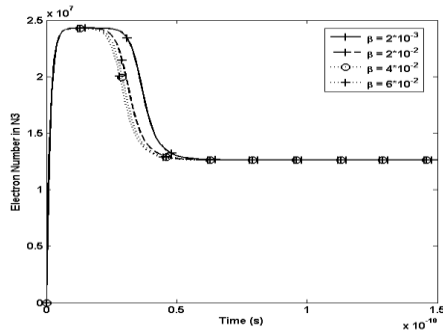


(b)

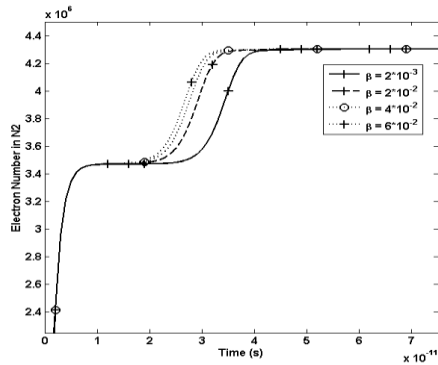
Fig. 6. a) Current vs Optical Power characteristics  
b) Current vs Optical Power characteristics (enlarged view around threshold current)

### 3.1.2 Time evolution characteristics

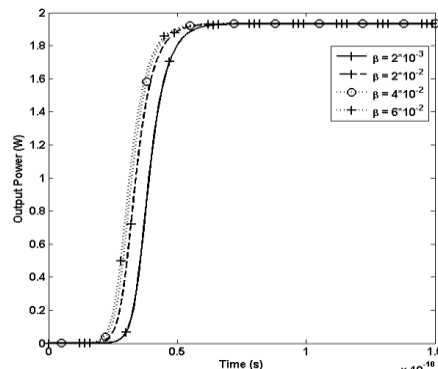
When a step current of  $2.5I_{th}$  is applied to the device, the variation of the parameters  $N_3$ ,  $N_2$  and transient optical power with respect to time are evaluated. The behaviour of  $N_3$  is such that it increases, reaches an initial steady state value of  $2.43 \times 10^7$  before falling off to the final steady state value of  $1.26 \times 10^7$  at around 75ps. It is seen that as the value of  $\beta$  is increased, the roll off rate of  $N_3$  remains same but the time taken to reach the final steady state value is significantly reduced. The larger the value of  $\beta$ , the lesser is the time taken for  $N_3$  to settle down to its final steady state value which is evident from Fig. 7a.



(a)



(b)



(c)

Fig. 7. a) Transient evolution of electron population in  $N_3$  b) Transient evolution of electron population in  $N_2$  c) Transient Power characteristics

As  $N_3$  decreases for a particular value of bias current,  $N_2$  and photon number show an increasing behaviour. As  $\beta$  value is varied,  $N_2$  attains steady state value of  $4.30 \times 10^6$  much quickly at around 35ps. The slope with which  $N_2$  increases to attain its steady state value for different values of  $\beta$  was almost found to be a constant value. This is demonstrated in Fig. 7b. The transient power characteristics also showed a reduction in rise time for increasing value of  $\beta$ . The steady state value of around 1.9W is attained at 75ps. The slope with which transient power reached steady state value was found to be constant when  $\beta$  was increased as in Fig. 7c.

### 3.1.3 Overall impact of ' $\beta$ '

When  $\beta$  is increased, as seen from the transient characteristics, the output power from the laser also increases linearly as shown in Fig. 8.

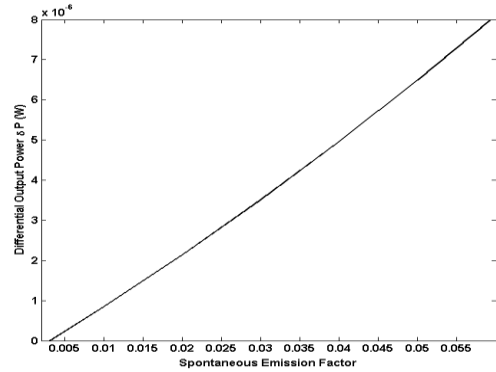


Fig. 8. Variation of Steady state differential output power vs  $\beta$

The built-up time is the time taken by the photon number to reach 10% of its steady state value from threshold. It can also be computed as the period when  $N_3$  is constant. It falls off nearly from 4 ps to 1 ps when  $\beta$  is increased, which is seen in Fig. 9.

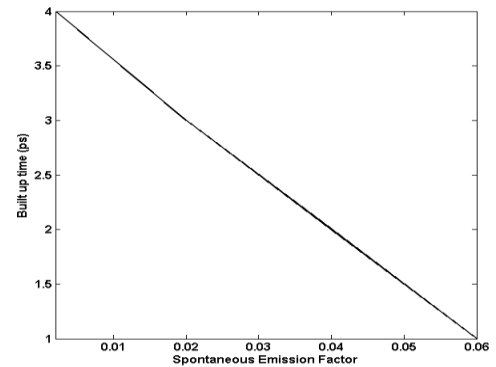


Fig. 9. Variation of Built-up time vs  $\beta$

The delay time is found to reduce from 30.3 ps to 23 ps, when  $\beta$  is increased. The variation is shown in Fig. 10.

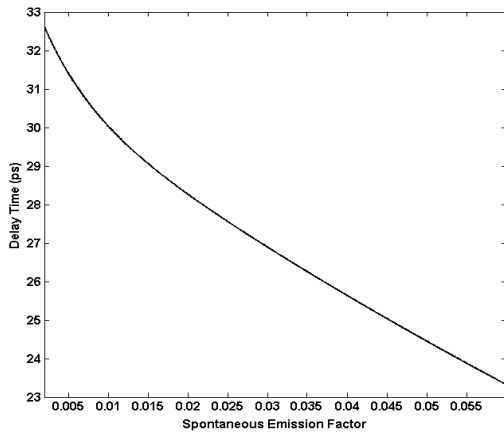


Fig. 10. Variation of Delay time vs  $\beta$

The rise time is computed as the time taken for the photon number to rise from 10% of its steady state value to 90% of its steady state value. It assumes wider significance as shares an inverse relationship with the bandwidth of the device. The rise time variation is observed to be very minimal.

It falls from 15.3ps to 14.5ps. The variation is shown in Fig. 11. It can also be asserted that as the rise time falls, the bandwidth of the device increases manifolds.

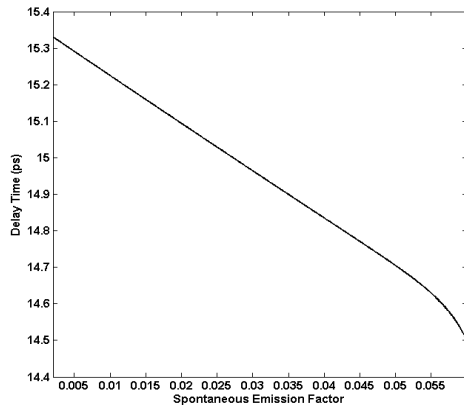


Fig. 11. Variation of Rise time vs  $\beta$

### 3.2 Influence of Optical Confinement Factor ( $\Gamma$ )

The optical confinement factor is defined as the fraction of the energy of a particular waveguide mode confined to the active region. It is also defined as the ratio of the light intensity within the active region to the sum of light intensity both within and outside the active region. The optical confinement factor is very important for a semiconductor laser having optical gain in the core region, as it relates to the modal gain. The optical confinement factor has a greater impact on the turn-on delay time. A good laser source design should maximize the optical confinement factor in the active layer. With a reasonable value, the pulse distortion can be reduced due

to the delay time, overshoot and relaxation oscillation effect of the response.  $\Gamma$  is basically modeled as a fitting parameter for the rate equations and by maximizing the value of  $\Gamma$ , we can expect a distortion free response from the laser as suggested in literature [20]. The optical confinement factor is varied from 0.25 to 0.45 in a uniform fashion with fixed values of  $\beta$  ( $2 \times 10^{-3}$ ), Reflectivity (0.29), and its effect on performance of QCL is studied.

#### 3.2.1 DC characteristics

The bias current ( $I$ ) to the QCL is varied from 0-2A and the optical power ( $P$ ) is calculated. The DC characteristic curve of the device is obtained by plotting  $I$  vs  $P$ . The dc characteristic curve starts shifting towards its left which is indicative of occurrence of reduction in threshold current. The slope variation ( $dP/dI$ ) is almost a constant for each value of  $\Gamma$  considered. The result is evident from Fig. 12. It is seen from the dc characteristic that threshold current decreases from 1.11A to 0.65A linearly as illustrated in Fig. 12. The optical power corresponding to a current of 2A, is found to increase linearly from 1.089W to 1.847W, owing to better optical confinement in the active region as depicted in Fig. 12.

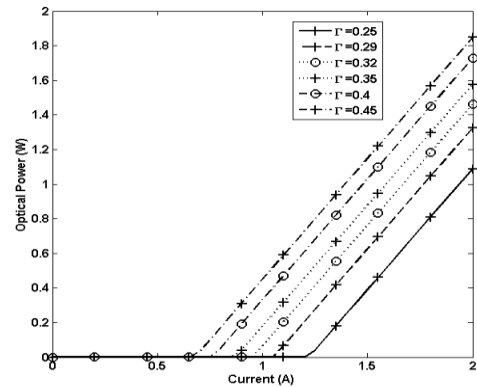


Fig. 12. Current vs optical power characteristics

#### 3.2.2 Time evolution characteristics

When a step current of  $2.5I_{th}$  is applied to the device, the variation of the parameters  $N_3$ ,  $N_2$  and transient optical power with respect to time are evaluated. It is seen that  $N_3$  increases linearly, attains an initial steady state value of  $2.43 \times 10^7$  before falling off to attain its final steady state value. As  $\Gamma$  is increased, the fall off rate is high such that the final steady state value is attained in a very less duration while the magnitude is reduced considerably. The lowest final steady state value is reached for the largest value of  $\Gamma$  as in Fig. 14a. The slope ( $dN_3/dt$ ) as found from the transient response curve increased from  $0.53 \times 10^6/\text{ps}$  to  $1.56 \times 10^6/\text{ps}$  as  $\Gamma$  is increased from 0.25 to 0.45 uniformly. The steady state value of  $N_3$  is achieved at around 100ps for each variation of  $\Gamma$ .

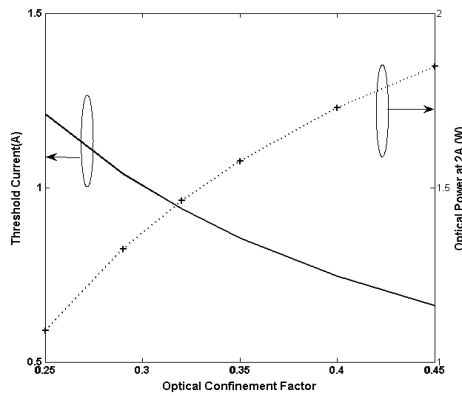
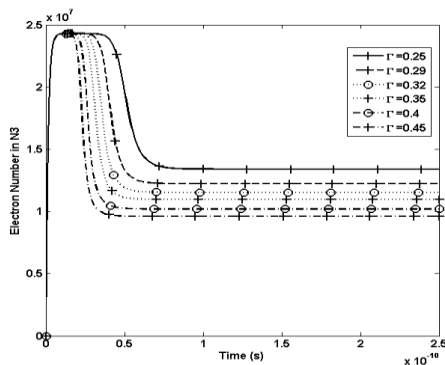
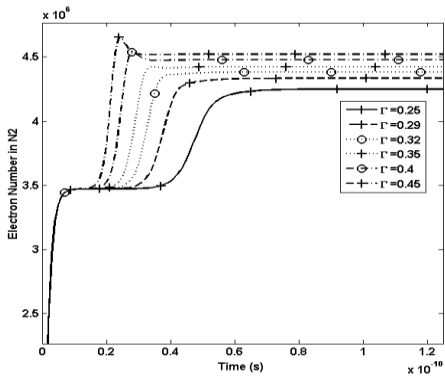


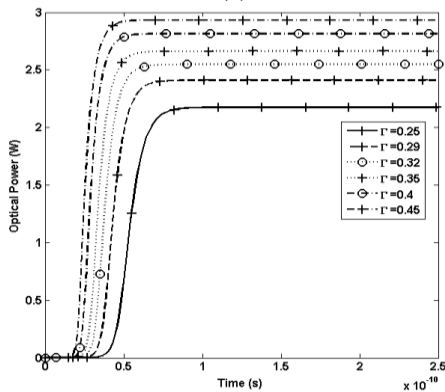
Fig. 13. Variation of Threshold Current and Output Power at 2A vs  $\Gamma$



(a)



(b)



(c)

Fig. 14. a) Transient evolution of electron population in  $N_3$   
 b) Transient evolution of electron population in  $N_2$   
 c) Transient power characteristics

As  $N_3$  decreases for a particular value of bias current,  $N_2$  and photon number show an increasing trend. As  $\Gamma$  value is varied,  $N_2$  attains higher steady state values for increasing values of  $\Gamma$  at around 60ps. Even the time taken by  $N_2$  to reach the steady state value is reduced considerably. It can be noted from Fig. 14b that there is a peak overshoot occurring for electron number in  $N_2$  when the optical confinement is maximum and it vanishes subsequently as the optical confinement is reduced from there on. This can be thought of underdamped oscillations occurring in a system when a step current is applied.

The same behaviour is also expected in the case of photon number which relates to transient optical power. As  $\Gamma$  is increased, the time taken by the optical power to reach its final steady value is reduced largely. One important point is worth stating here is that highest steady state optical power is obtained for highest value of  $\Gamma$  in a much quicker time as seen in Fig. 14c. It is evident from the graph that the curves shift leftwards indicating the fact that the rise time is reduced leading to an increased bandwidth of operation of the device.

### 3.2.3 Overall impact of ' $\Gamma$ '

When  $\Gamma$  is increased,  $N_3$  decreases from a steady state value of  $1.34 \times 10^7$  to  $0.96 \times 10^7$  which closely approximates to an exponential decay as in Fig. 15. A reciprocal variation with respect to  $N_3$  is observed for  $N_2$ . It increases from  $4.25 \times 10^6$  to  $4.52 \times 10^6$  in an almost linear manner as in Fig. 14. This is also evident from the dc characteristics where  $N_3$  attained lower steady state values as the confinement factor was increased while  $N_2$  and the photon number showed an increasing trend.

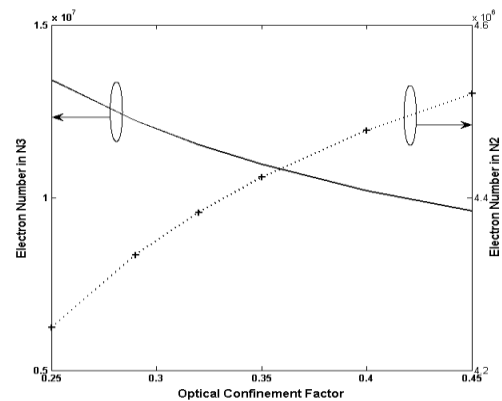


Fig. 15. Variation of Steady State electron population in  $N_3$  and  $N_2$  vs  $\Gamma$

The built-up time, rise time and delay time curves are found to exhibit exponential decay characteristics. The method of computing these time parameters has been discussed earlier and the variation of these parameters with respect to  $\Gamma$  logically matches with the dc and the transient characteristics of  $N_3$ ,  $N_2$  and power as in Fig. 16.

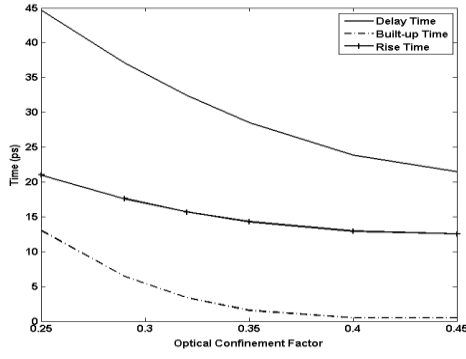


Fig. 16. Variation of Delay time, Built up time, Rise time vs  $\Gamma$

### 3.3 Influence of mirror reflectivity

The photon life time and reflectivity are related by Eq. (10)

$$\tau_p^{-1} = \frac{c}{n_{eff}} (\alpha_w + \alpha_m) \quad (10)$$

where  $\alpha_w$  is the waveguide loss of the cavity while  $\alpha_m$  is the mirror loss expressed in Eq. (11).

$$\alpha_m = \frac{-\ln(R_1 R_2)}{2L} \quad (11)$$

$R_1$  and  $R_2$  are the reflectivities of facets 1 and 2 respectively;  $n_{eff}$  is the refractive index of the cavity and  $c$  being the velocity of light in free space. The reflectivity is varied from 0.25 to 0.45 keeping  $\beta$  fixed at  $2 \times 10^{-3}$  and mode confinement factor at 0.32.

#### 3.3.1 DC characteristics

The bias current ( $I$ ) to the QCL is varied from 0-2A and the optical power ( $P$ ) is calculated. It is evident from the graph as in Fig. 17 that the threshold current reduces gradually and an increased power output is observed. The slope ( $dP/dI$ ) decreases from 1.174 W/A to 1.0419 W/A as the reflectivity is increased uniformly. It is worth mentioning to quote that the slope variation is not uniform as in Fig. 16 and a reduction in slope is expected.

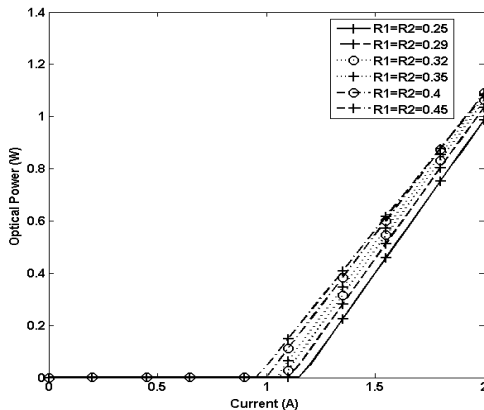
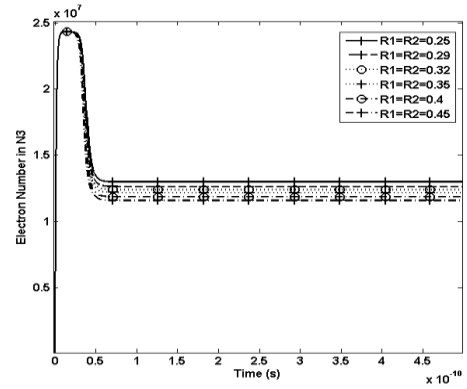


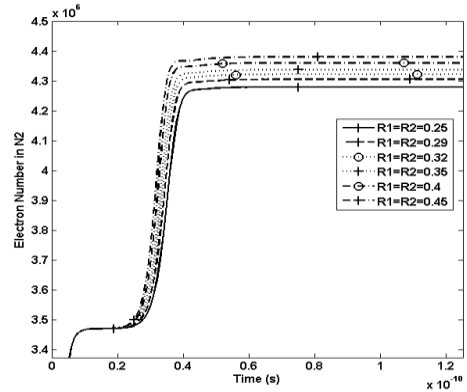
Fig. 17. Current vs optical power characteristics

#### 3.3.2 Time evolution characteristics

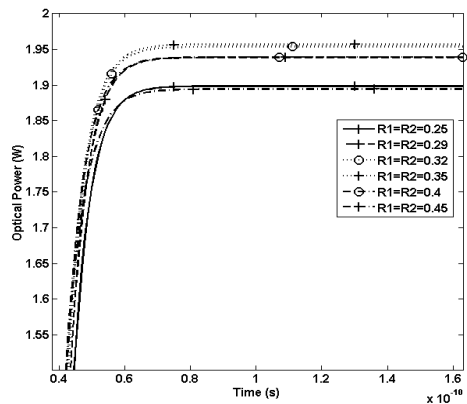
When a step current of  $2.5I_{th}$  is applied to the device, the variation of the parameters  $N_3$ ,  $N_2$  and transient optical power with respect to time are evaluated. It is seen that  $N_3$  increases linearly, attains an initial steady state value of  $2.43 \times 10^7$  before falling off to its final steady state value at around 75ps. The initial steady state value is almost constant and the fall off rate is also uniform and equal for all values of reflectivities.  $N_3$  attains lowest final steady state value for highest value of Reflectivity as depicted in Fig. 18a.



(a)



(b)



(c)

Fig. 18. a) Transient evolution of electron population in  $N_3$   
b) Transient evolution of electron population in  $N_2$  c)  
Transient power characteristics

As the step current is applied,  $N_2$  shows an increasing behaviour and it attains increased steady state value at a lesser time for higher reflectivities as in Fig. 18b. At around 50ps, all the curves of  $N_2$  attain their respective steady state values. The same is observed with transient power. It increases with increasing values of reflectivity and attains steady state value more quickly resulting in increased output power as in Fig. 18c. At around 70ps, the different curves of transient power attain their steady state value.

### 3.3.3 Overall Impact of 'R'

The steady state value of  $N_3$  is a linearly decreasing function of reflectivity while it is an increasing function for  $N_2$  which can be justified from the transient time evolution curves as in Fig. 19.

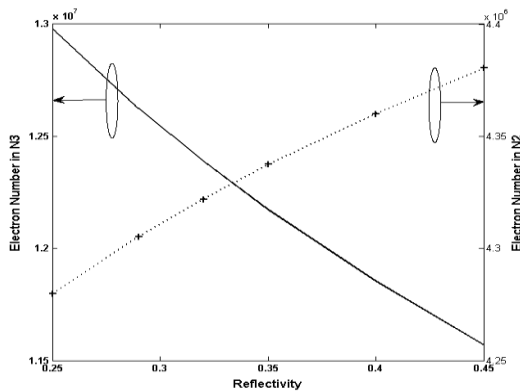


Fig. 19. Variation of Steady State electron population in  $N_3$  and  $N_2$  vs Reflectivity

The threshold current is observed to be a linearly decreasing function of reflectivity. It reduces from 1.15A to 0.95 A while the optical power increases from 0.9862W and then saturates to a steady state value at 1.092W for higher values of reflectivity as in Fig. 20. The photon life time variation is also found to be a linear function of reflectivity as in Eq. 10. A similar behaviour is observed from Fig. 21.

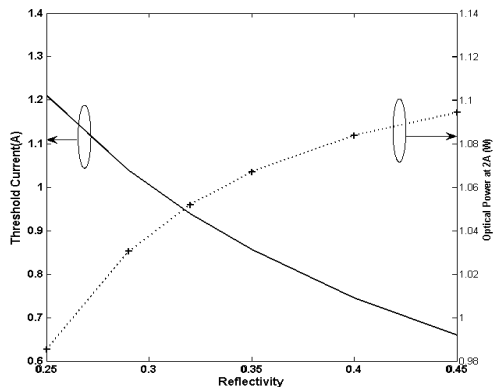


Fig. 20. Variation of Threshold Current and Output Power at 2A vs Reflectivity

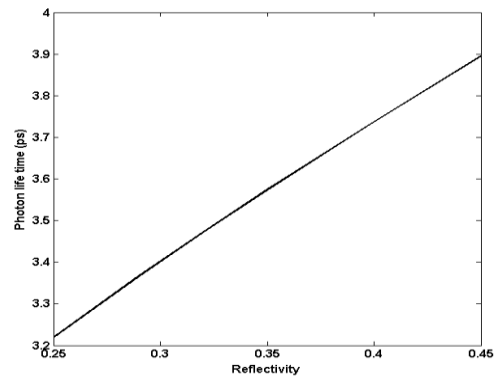


Fig. 21. Variation of Photon life time vs Reflectivity

The delay time characteristics of the device showed a slight variation and it falls off exponentially from 33.5ps to 30.7ps in a linear fashion. It justifies that the delay time reduces because it takes lesser time for  $N_2$  and the photon number to reach their respective steady state values. The rise time falls off rapidly from 28.5ps initially but to settle at 15.4ps, as illustrated in Fig. 22. A significant fall in rise time indicates the increased bandwidth of the device.

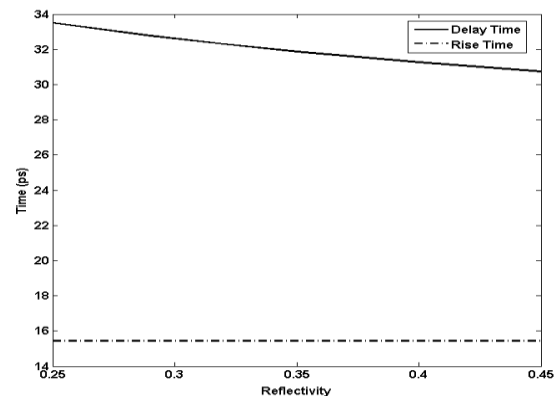


Fig. 22. Variation of Delay time and Rise time vs Reflectivity

## 4. Conclusion

In this work, the influence of mode confinement factor, spontaneous emission factor and mirror reflectivity on the QCL device behaviour have been examined. The rate equations were solved using MATLAB®, for DC and dynamic characteristics under different values of device parameters. When the spontaneous emission factor was varied, non linearity was observed in the P-I characteristics around the threshold current region. A peak overshoot was observed in  $N_2$  when optical confinement factor was highest which subsequently vanished as the factor was lowered. There were slope variations visibly seen in  $N_3$ ,  $N_2$  as the factor was varied. Slope variations were observed in P-I characteristics when reflectivity was varied. While all the parametric variations are studied, a common phenomenon was observed. Threshold current was reduced and an increased output power is clearly seen. The built-up time,

delay time and rise time exhibited an exponential reduction from their initial values.

## References

- [1] J. Faist, F. Capasso, D. L. Sivco, C. Sirtori, A. L. Hutchinson, A. Y. Cho, Quantum cascade laser, *Science*, **264**, 553(1994).
- [2] H. Page, C. Becker, A. Robertson, G. Glastre, V. Ortiz, C. Sirtori, *Applied Physics Letters*, **78**, 3529 (2001).
- [3] W. H. Ng, E. A. Zibik, M. R. Soulby, L. R. Wilson, J. W. Cockburn, H. Y. Liu, M. J. Steer, M. Hopkinson, *Journal of Applied Physics*, **101**, 046103 (2007).
- [4] G. Scamarcio, F. Capasso, C. Sirtori, J. Faist, A. L. Hutchinson, D. L. Sivco, A. Y. Cho, *Science*, **276**, 773 (1997).
- [5] S. Anders, W. Schrenk, E. Gornik, G. Strasser, *Applied Physics Letters*, **80**, 1864 (2002).
- [6] D. Hofstetter, M. Beck, T. Aellen, J. Faist, *Applied Physics Letters*, **78**, 396 (2001).
- [7] J. Faist, M. Beck, T. Aellen, E. Gini, *Applied Physics Letters*, **78**, 147 (2001).
- [8] C. Walther, G. Scalari, J. Faist, H. Beere, D. Ritchie, *Applied Physics Letters*, **89**, 231121 (2006).
- [9] Chang Qi, Xinzhi Shi, Shuangli Ye, Jinguang Jiang 2013 IEEE International Conference of Electron Devices and Solid-State Circuits (EDSSC), **0**, 1 (2013).
- [10] Chang Qi, Xiaojun Xia, Xinzhi Shi, Shuangli Ye, 2013 IEEE International Conference of Electron Devices and Solid-State Circuits (EDSSC), **0**, 1(2013).
- [11] Wei Zhou, Shaobin Liu, Jie Wu, Xiaoliu Zhang, Wu Tang, *Quantum Electronics*, **4**, 289 (2014).
- [12] J. F. Webb, M. K. Haldar, *Journal of Applied Physics*, **111**, 043110 (2012).
- [13] A. Hamadou, S. Lamari, J. L. Thorbel, *Journal of Applied Physics*, **105**, 093116 (2009).
- [14] Kelvin S. C. Yong, Manas K. Haldar, Jeffrey F. Webb, *Journal of Infrared Milli Terahz Waves*, **34**, 586 (2013).
- [15] Rodney S Tucker, *IEE Proceedings on Solid State and Electron Devices*, **128**, 180 (1981).
- [16] S. Piramasubramanian, M. Ganesh Madhan, *J. Optoelectron. Adv. M.* **16**, 93 (2014).
- [17] M. Ganesh Madhan, P. R. Vaya, N. Gunasekaran, *IEEE Photonics Technology letters*, **11**, 27 (1999).
- [18] G. P. Agrawal, N. K. Dutta, Co, Inc, Newyork (1986).
- [19] Peter Hering, Jan Peter Lay, Sandra Stry, Springer-Verlag Berlin Heidelberg (2004).
- [20] Le Nguyen Binh, CRC press, Boca Raton (2015).

---

\*Corresponding author: ashokp2k4@gmail.com